# Design and implementation of a dexterous anthropomorphic robotic typing (DART) hand



2011 Smart Mater. Struct. 20 035010

(http://iopscience.iop.org/0964-1726/20/3/035010)

Smart Mater. Struct. **20** (2011) 035010 (12pp) doi:10.1088/0964-1726/20/3/035010

# Design and implementation of a dexterous anthropomorphic robotic typing (DART) hand

**Nicholas Thayer and Shashank Priya**[1]

Center for Intelligent Material and Systems (CIMSS), Center for Energy Harvesting Materials and Systems (CEHMS), Virginia Polytechnic Institute and State University, Blacksburg, VA 24061, USA

E-mail: spriya@vt.edu

Received 20 July 2010, in final form 10 January 2011
Published 9 February 2011
Online at stacks.iop.org/SMS/20/035010

**Abstract**
This paper focuses on design and implementation of a biomimetic dexterous humanoid hand. Several design rules are proposed to retain human form and functionality in a robotic hand while overcoming the difficultly of actuation within a confined geometry. Size and weight have been optimized in order to achieve human-like performance with the prime objective of typing on a computer keyboard. Each finger has four joints and three degrees of freedom (DOF) while the thumb has an additional degree of freedom necessary for manipulating small objects. The hand consists of 16 servo motors dedicated to finger motion and three motors for wrist motion. A closed-loop kinematic control scheme utilizing the Denavit–Hartenberg convention for spatial joint positioning was implemented. Servo motors housed in the forearm act as an origin for wires to travel to their insertion points in the hand. The dexterity of the DART hand was measured by quantifying functionality and typing speed on a standard keyboard. The typing speed of a single DART hand was found to be 20 words min$^{-1}$. In comparison, the average human has a typing speed of 33 words min$^{-1}$ with two hands.

(Some figures in this article are in colour only in the electronic version)

## 1. Introduction

The evolution of a body part is primarily based on the demands placed on it by the environment. Hooves, claws, fins and hands are examples of anatomical structures that provide mobility and survival capability. A range of designs for these body parts can be found in Nature, each showing the effect of species anatomy and the environment in which it survives. For example, primates often have five fingered hands similar to that of a human but each species has optimized a different method for utilizing this appendage. Some species have developed tough skin above the knuckles in order to walk on all four limbs, while others have developed long slender fingers that assist with grasping tree branches. The human hand, with roughly 17 000 nerve endings [1], has evolved to take advantage of the precision grasp where the fingertips are used in conjunction with the thumb to precisely manipulate objects. But as human society has evolved so has the demand placed on it by the environment. Human hands also communicate complex ideas and emotions on top of being highly dexterous. In 1834, Charles Bell [2] wrote: 'and we must confess that it is in the human hand that we have the consummation of all perfection as an instrument'. It is natural for a researcher to create a dexterous manipulator that mimics the human hand since its inherent capabilities can be observed in their own hand. In order to implement these characteristics into a robotic hand, several innovations are required. We list here some of the efforts made in this direction by the research community.

- Gifu hand III [3]. Developed as a prosthetic device, this hand is driven with servo motors, has 16 degrees of freedom (DOF), five fingers, underactuation through four-bar linkages and a large area tactile sensor.
- Utah/MIT hand [4]. Utilizes 32 pneumatic actuators to drive three fingers and a thumb through a system of

[1] Author to whom any correspondence should be addressed.

 

cables. A dense sensing system is integrated with vision to perform trajectory planning.

- DIST hand [5]. Utilizes Bowden cables to provide extrinsic actuation to a four fingered 16 DOF hand with 20 brushless DC motors (BLDC). Fingertip force, joint angle and a novel conductive rubber tactile sensor greatly increase the sensing capability of this hand.
- DLR hand II [6]. This 16 DOF, four fingered hand is driven with 13 BLDC motors with underactuation provided by a four-bar linkage of two distal joints. Over 90 sensors and an impressive electronics packaging give this hand great potential for conducting research.
- RCH-1 [7]. This ultra-light (320 g), 16 DOF hand was intended for prosthetics. High underactuation through a passive cable–pulley system allows control of five fingers with six BLDC motors.
- Blackfingers prosthetic [8]. Thirty-one pneumatic cylinders control the 23 DOF in an antagonistic cable setup that almost completely mimics the skeletal structure of the human hand.
- SHADOW hand. Developed by Shadow Inc., uses 20 air muscles to fluidly actuate five fingers (21 DOF) and a two DOF wrist. This is one of the more dexterous hands because of the 'folding palm' structure.
- Robonaut hand [9]. Created by NASA, uses 14 BLDC motors to control 14 DOF. Flex shafts and lead screw assemblies are used instead of cables to eliminate frictional problems. Two fingers have a single DOF for grasping, which reduces the minimum number of motors, and three fingers have three DOF for precision manipulation. With the addition of 42 integrated sensors, this is a robust tool for tasks in space.

Slight changes in hand design from others, such as fins or claws, enable us to write, open doors, tie knots and perform many other 'activities of daily living' (ADLs). Since the human hand is a naturally engineered biomechanical system it poses several design challenges in its replication, often leading to simplifications that degrade performance. A change in architecture of the hand would result in different control schemes for performing ADLs and thus would no longer represent the functionality of the human hand. Therefore in trying to mimic the functionality of the human hand it is important to mimic its musculoskeletal structure. Here lies a fundamental problem between engineering and evolution: there are no actuators which can provide performance akin to that of natural muscles. Recent studies by Tadesse *et al* [10] as well as Thayer *et al* [11] present a comparative analysis of currently available actuation technologies and artificial muscles. By using cost function analysis based on strain, pressure, energy density and efficiency, a number of viable electroactive polymers (conducting polymers, SMP, NiTi SMA, acrylic and silicone dielectric elastomers, single crystal PZN-PT, and MFC) have been selected for robotic applications. Single crystal PZN-PT, MFC, silicone and acrylic dielectric elastomers were eliminated due to high voltage requirements (>250 V) which made the driving electronics cumbersome. Shape memory polymer (SMP) and most conductive polymers were excluded for either slow response times (>20 s) or low efficiencies (<1%), thus leaving NiTi SMA as the electroactive polymer of choice. Disadvantages still remain in terms of electrical isolation, slow thermal responses, heat generation, hysteresis and difficulties with precise control. Thus traditional magnetic motors with relatively low voltage and power requirements, fast response times and ease of control are still the most viable solution.

In several cases, human-like dexterity is not needed to accomplish a goal. For example, Prosimians (lemurs and lorises) possess only a single prehensile pattern—the hand opens and closes like the jaws of a toy crane in an amusement arcade [12]. Industrial robots are designed for a specific job, exhibiting high dexterity in task-oriented pre-programmed applications in structured scenarios but exhibit low levels of anthropomorphism and manipulation capability [7]. However, in ADLs such as typing or opening doors many levels of dexterity becomes very important. In the past decades, due to a lack of high power density actuators suitable for prosthetics, mechatronic developers have basically focused on underactuated mechanisms design [13]. Underactuation is a term that describes a system with more degrees of freedom (DOF) than degrees of mobility (DOM), or more joints than actuators. The benefit of an underactuated design is the reduced number of actuators and overall size of the system while retaining some degree of functionality. Some of the most advanced prosthetic devices utilize superficial electromyographic (EMG) signals to drive motors for grasping [14–16]. The trouble with using these signals is that it is hard to distinguish readings from different muscles that are physically near to each other. Because of this, most prosthetics controlled by EMG signals have one or two actuators and a high degree of underactuation.

The objective of this study is to design, fabricate and control a dexterous robotic hand and wrist that acts as a communication interface between human and computer. The dexterity of this hand was quantified in terms of typing speed on a standard computer keyboard because it requires similar, if not more, dexterity compared to most other ADLs. This hand is intended to be integrated with humanoid robots that may eventually assist the elderly or disabled people with their activities of daily living such as opening doors, reaching objects, typing on a keyboard and movement assistance. These are simple tasks for a human to perform but the interaction between the brain, senses and muscle motion in the human body is very difficult to replicate in robotics.

## 2. Design of the humanoid hand

### *2.1. Actuator selection*

We started by investigating the human hand physiology to gain an understanding of its musculoskeletal structure and how it contributes to overall functionality. Metrics commonly used to quantify various aspects of hand design are size, weight, form, degrees of freedom, range of motion, grasp speed, and grasp force. Roughly 40 muscles are responsible for 23 degrees of freedom in the human hand and wrist, many existing to stabilize and connect biological tissue. Understanding

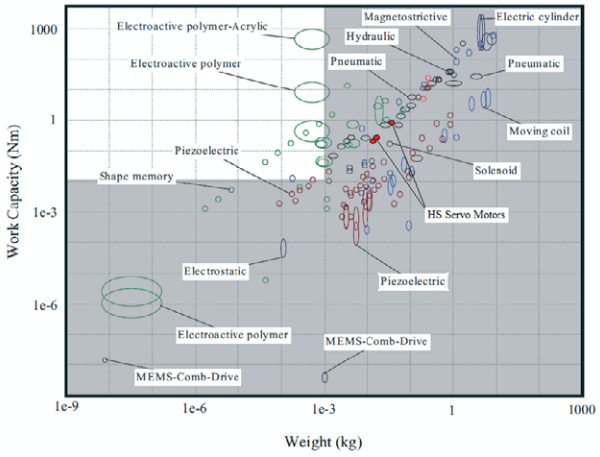


**Figure 1.** A plot of actuator work capacity versus mass including actuators chosen for the DART hand. Taken from [32]. Copyright Wiley-VCH Verlag GmbH & Co. KGaA. Reproduced with permission.

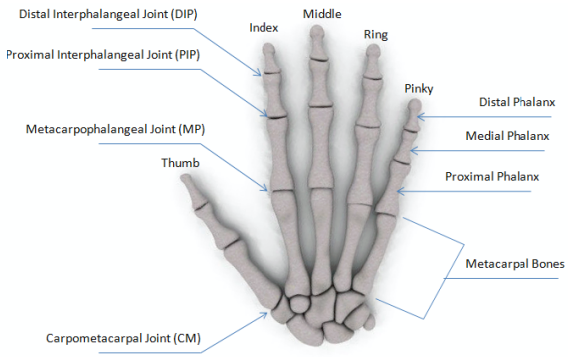


**Figure 2.** Skeletal nomenclature of the human hand.

which elements of the human hand are responsible for specific functions will help in eliminating unnecessary elements from the design, therefore reducing redundancy and complexity. With this mindset we build a model of the hand using CAD and a dynamic simulation program. Actuators were selected based on volume, strength and price, and were then integrated into the CAD model. To verify the design, fusion layer deposition rapid prototyping was used to create the prototypic system with ABS plastic. Several actuators such as pneumatics, hydraulics, BLDC motors, servo motors, air muscles, shape memory alloy and electroactive polymers were considered. Pneumatics and hydraulics were eliminated from consideration due to their bulky system requirements like regulators, filters and tanks. Air muscles were eliminated due to their size and difficulties with control stemming from highly nonlinear behavior. Shape memory alloys and most electroactive polymers were eliminated either due to low efficiencies, high voltage requirements or low output force, thus leaving BLDC motors or servo motors as the most viable solution. BLDC motors tend to provide more torque for their weight and volume especially with high gear reduction, however they are expensive. Thus, cost-effective (less than \$35/motor) servo motors with reasonable work density ($\sim$18 kJ m$^{-3}$) were selected as the suitable actuators. Figure 1 shows a comparison of weight to work capacity of many commonly used actuators as well as the HS servo motors chosen for the hand being developed in this study, henceforth referred to as the 'DART hand'.

### 2.2. Finger design

The human hand consists of a complicated set of muscles, bones, tendons, cartilage and ligaments that interact fluidly to produce efficient motion and high output forces. Figure 2 shows the bone structure and corresponding joint names for the human hand. The metacarpophalangeal (MP) joints are condylar joints which create two axes of motion, one more axis of motion than found in the DIP and PIP joints. The carpometacarpal (CM) joint of the thumb is a saddle joint, similar to the condylar joint, but with a greater range of motion, and is responsible for thumb opposition. These joints are replicated in the DART hand as universal joints which also create two axes of motion. The difference between artificial and biological joints is that a universal joint is rigidly locked in place at the intersection of the axes of rotation while human finger joints consist of concave and convex portions of cartilage that rest on each other and remain in place due to tension in passive and active tissue. The remaining joints in the human finger are hinge joints which allow motion about only one axis and are replicated in the DART hand as pin joints that behave similarly. The humanoid hand has 19 DOF broken down into three per finger, four for the thumb and three for the wrist.

The human finger represents a kinematic linkage system with nonorthogonal, nonintersecting axes of rotation at the CM and MP joints [17]. A system like this is difficult to model because the axes of rotation in human fingers constantly change with respect to joint angle [7]. Modeling the IP joints as orthogonal joints with a fixed axis of rotation and MP joints as two orthogonal intersecting axes of rotations does not significantly change the system's kinematics. Plane joints between the carpal bones in the wrist are ignored and the wrist is modeled as three orthogonal intersecting axes of rotation.

Muscle groups assisting more than one degree of freedom in a single finger are a property of the human hand that improves grip strength and finger stability. Muscles like the flexor digitorum superficialis, which are primarily responsible for flexion of the proximal interphalangeal (PIP) joint, flex the DIP joint as well as the MP joint at some level of contraction. By excluding this feature from the DART hand, grip strength, stability and system complexity will decrease but not to a point where the hand is unable to perform all necessary ADLs.

Independent control of each finger is also a feature of the DART hand that greatly reduces complexity. Muscles such as the flexor digitorum profundus, which are responsible for flexion of the distal interphalangeal (DIP) joint, are sometimes connected at the tendons and function to move joints in more than one finger (noticeable when one tries to flex the fingertips of the ring and pinky fingers independently). Removing this constraint increases the uniformity of the hand and reduces complexity in fabrication and control without sacrificing functionality.

An underactuated system has more DOF than DOM. Many underactuated robotic hands have been developed [18–21], some utilizing four-bar mechanisms while others use differential mechanisms to passively grasp objects. The TUAT/Karlsruhe hand [22] uses a single actuator to drive a multi-fingered differential hand for passive grasp shaping. The DART hand uses a modified version of the underactuated four-bar mechanism of the TUAT/Karlsruhe hand to couple the DIP and PIP joints. The design benefits of a four-bar mechanism include rigid joint connections and the removal of an actuator per finger. This mechanism permits 70° rotation for the DIP joint and 90° for the PIP joint, whereas the human finger can achieve 70° and 110° respectively. Since thumb dexterity is important in fine manipulation tasks it does not incorporate this four-bar mechanism thus leaving independent control of each joint. A universal joint connects the thumb to the palm and allows the thumb to touch each fingertip as well as the opposing end of the palm.

Human hands have separate muscles for flexion and extension. Sometimes both sets of muscles actuate to help with stability, but as mentioned before this function has been removed from the DART hand. Torsional springs placed at the joints eliminate the need for extensor muscles thus removing the need for these motors. Figure 3(a) shows the CAD model of the finger mechanism built using Unigraphics 6.0. The MP adduction/abduction joint axis is perpendicular to the joint axis for flexion/extension (not shown in figure 3(a)). A rectangular block fits between the palm and proximal phalanx and is held together with pins which create a universal joint. An important feature is the tunnel that routes the wires from the dorsal (palm) to the ventral (back) side of the hand. As the IP joints are flexed, extensor muscles are activated to keep other joints from also flexing. Since there are no extensor motors in the artificial hand the force experienced from IP joint flexion would overcome the holding force of the torsional springs and cause the MP joint to co-flex. Some designs take advantage of this feature to create a shape-forming grasping mechanism as mentioned earlier. To remedy this, IP joint wires are routed to the ventral (back) side of the finger to stabilize the flexion motion against the wire responsible for MP joint flexion much like opposing stabilizing cables on a radio tower.

In order to maintain human-like function and range of motion, the kinematics of the four-bar mechanism linking the DIP and PIP joints should mimic those of a human. A four-bar mechanism can produce trajectories through various link lengths and pin locations. Figure 3(b) shows the finger link mechanism. To reach this configuration, the positions of the pin joints and link lengths were varied until the trajectory of the fingertip during flexion remains within 3 mm of a human fingertip trajectory at all times. The multi-body dynamic simulation program ADAMS was used to simulate and measure the trajectory of the robot's fingertip, as shown in figure 4(a). To compare the trajectories of the robot to a human, position data from a participant's finger was collected with a high-speed camera. A program developed using MATLAB tracks and plots reflective points at the fingertip and IP joints on the participant's finger as it flexes as shown in figure 4(b). A comparison between human and robot is shown in figure 4(c)

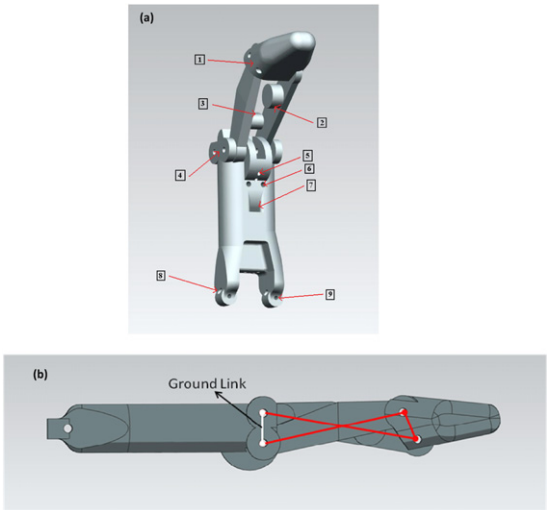


**Figure 3.** (a) Structure and functional elements of a finger of the DART hand. The arrows in this figure point to important design features such as: (1) DIP joint axis, (2) insertion point for IP joint motion, (3) attachment point for torsional spring on middle phalanx, (4) PIP joint axis, (5) attachment point for torsional spring on proximal phalanx, (5) insertion point for flexion/extension MP joint motion, (6) tunnel to route wires from dorsal (palm) to ventral (back) side of hand, (7) MP joint axis for flexion/extension, (8) insertion point for adduction/abduction MP joint motion, (b) four-bar mechanism created by the medial phalanx links.

that clearly reveals that the trajectory is within 3 mm of the human finger at all times and the difference at the end of the trajectory is 1.5 mm.

It is known that an average peak force of 2 N is experienced while typing [23]. Unlike other nonprehensile skills like piano playing, striking a key with more force does not affect the input to a computer. During typing, force is a rather loosely controlled variable that is programmed simply to exceed the activation force of the key [23]. Figure 5 shows the fingertip force normalized to the maximum output of the actuators versus joint angle for the given finger geometry. Flexion of the PIP joint was accomplished with the HS-85MG servo motors with a maximum output torque of 34.6 N cm. The moment arm from the motor horn was 1.1 cm which creates a maximum linear force of 31.5 N leading to a maximum fingertip force of 12.1–14.4 N. The HS-225BB motor was used to flex the MP joint and provide a maximum fingertip force of 12–17.3 N. Since the PIP joint is the limiting factor, a maximum fingertip force range of 12.1–14.4 N was achievable without stalling the HS-85 motors.

### *2.3. Wrist and forearm design*

The MP joints (or knuckles) of the artificial hand were offset from each other at average distances and angles as depicted in [24]. Other dimensions like finger length, palm size, finger spacing and forearm size were also optimized to be within the statistical average. Keeping the dimensions of the artificial hand similar to those of an average person is important, especially for keyboard typing, since slight deviations in dimensions will affect the user's ability to utilize a keyboard.

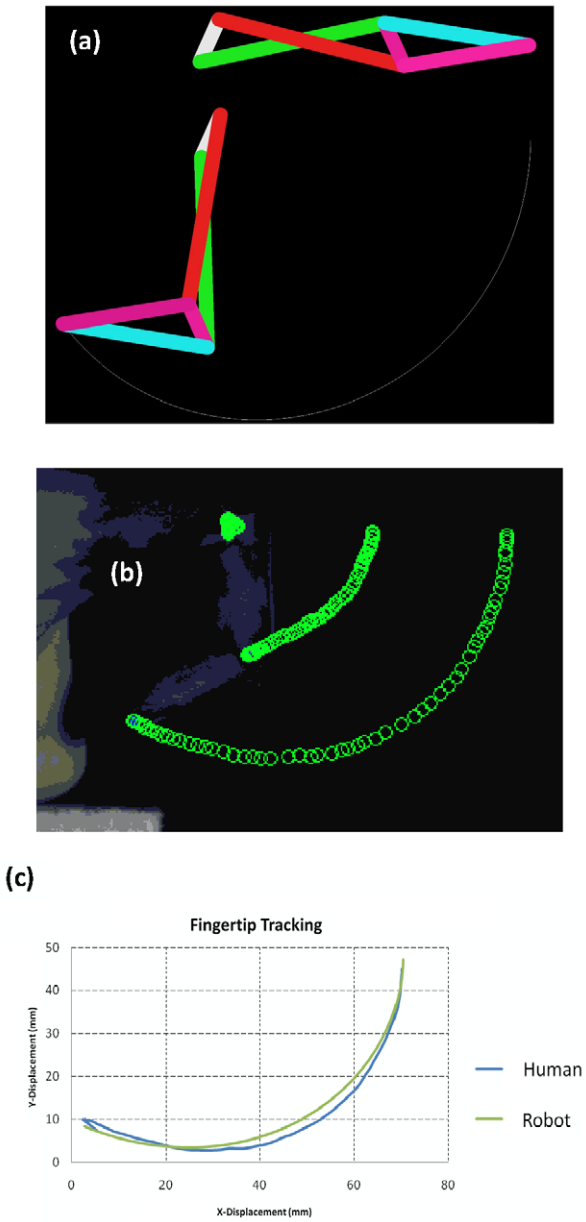


**Figure 4.** (a) Fingertip trajectory analysis carried out with ADAMS, (b) tracking reflective points on a human finger with a high-speed camera and MATLAB, and (c) fingertip trajectory comparison between the human participant and the robot. The robot maintained a maximum offset of 3 mm from the human finger at all times.

For example, if the palm is proportionally larger to the fingers the wrist will have to compensate for this length by extending until the resting position of the fingers reaches the center row keys. The shoulder and elbow can also be used to move the position of the entire hand with respect to the keyboard to compensate for this disproportion but will add unnecessary complexity and cost.

Finger flexion, abduction and adduction are provided by high tensile strength wires that originate from servo motors in the forearm, as shown in figure 6(a), and run to insertion points on the fingers. This replicates the natural function of extrinsic muscles in the human forearm. The forearm is composed of four modules that house the motors and provide

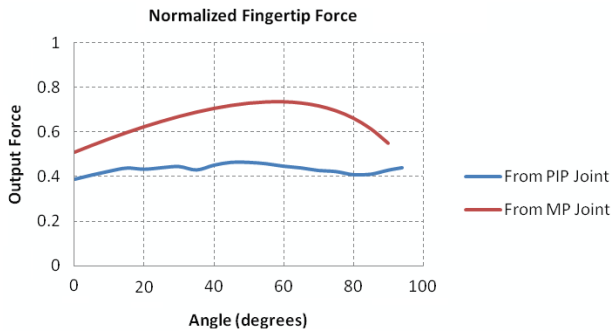


**Figure 5.** Percentage of maximum motor output experienced at the fingertip. PIP joint rotation produces less force at the fingertip and is therefore the limiting value for maximum fingertip force.

a support structure. Two motors are placed near the hand to control the wrist and every succeeding module houses motors to actuate the fingers and thumb. Smaller motors are placed closer to the hand to reduce the moment arm for a future elbow mechanism. Between the last two modules is the Lynxmotion SSC-32 servo motor controller that is used to distribute pulse commands and amplify signals to the motors. At the end of forearm is a cover that houses a motor and gearbox for rotation of the entire forearm, mimicking the ulna and radius crossover in a natural human arm, as shown in figure 6(b). A holding bolt runs through a central gear, cover plate, and thrust bearings attaching to a stationary elbow assembly. This mechanism allows 110° of rotation while a human is able to rotate their forearm roughly 150°. Pictures of the fabricated DART hand are compared with the human hand in figures 6(c) and (d). The DART hand has been designed slightly smaller than average to account for silicone skin that will cover the entire skeletal structure of the hand and upper forearm, as shown in figure 6(e). The skin helps with the gripping friction and also increases the resemblance to a human hand. Future improvements to the design will include a similar skin with embedded piezoelectric sensors to assist with tactile sensing.

The tendons that travel in a human hand pass through the carpal tunnel which acts as a protective sheath and keeps them from separating from the wrist like a string on a bow. The tendons that actuate the human wrist originate in the forearm and insert on the carpal bones to flex and extend the hand. The humanoid wrist utilizes a differential mechanism that combines inputs from two servo motors to rotate about two axes. Instead of using wires which are only capable of pulling, the humanoid wrist uses two rigid rods to push and pull, creating a combined moment about the wrist. To flex or extend, both motors move forward or backward, and to adduct or abduct, the motors move opposite to each other. The carpal tunnel was replaced with a universal joint that allows the wires in the fingers to pass through it. A picture of the fabricated wrist mechanism is shown in figure 7(a).

In the human wrist, tendons run from muscles in the forearm through the carpal tunnel to their insertion points in the hand. When the wrist rotates some tendons experience tension while others gain slack. Natural elasticity in the human body reduces some of these effects and the brain compensates for

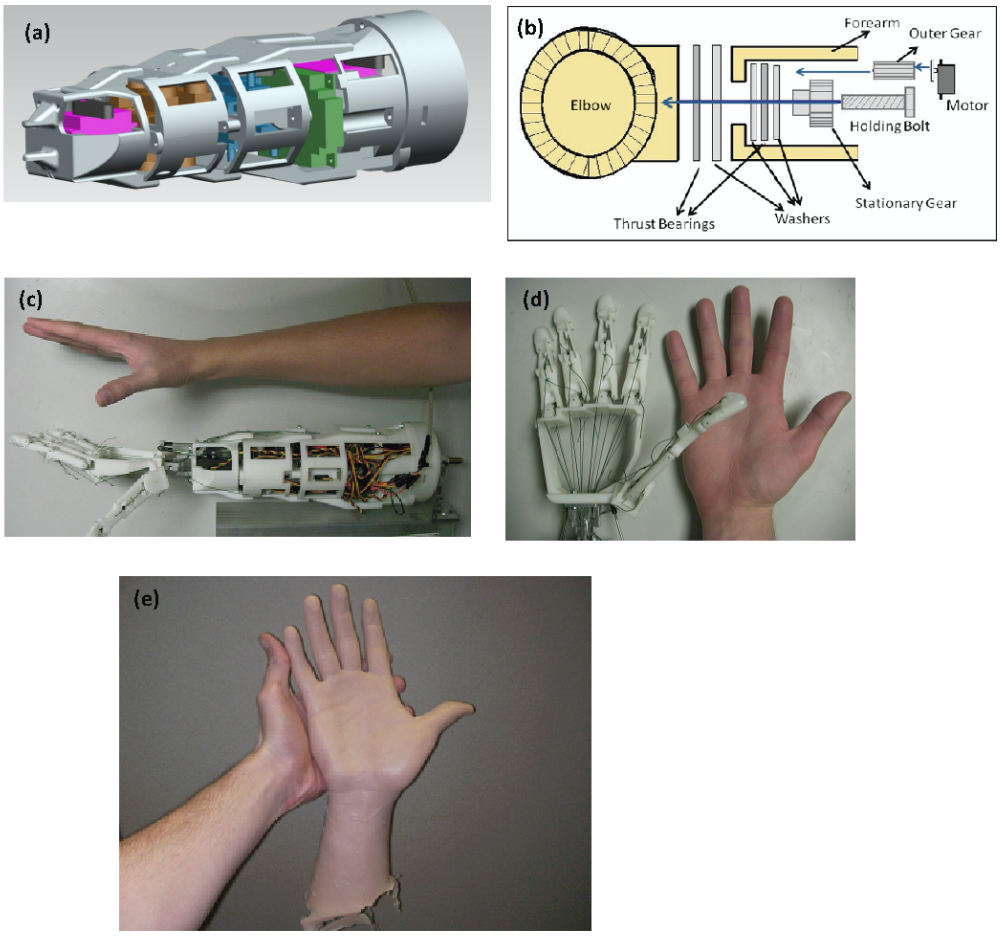


**Figure 6.** (a) CAD file of the forearm showing the electronics and 18 of the 19 motors. (b) Mechanism developed for rotation of the entire forearm. (c) Visual comparison of the robotic forearm to a human forearm. (d) Visual comparison of the DART hand to a human hand, and (e) hollow silicone skin covers the mechanical components of the DART hand.

any additional forces by contracting other muscles. However, in a robotic system, which is rigid, any extra slack or tension will cause unwanted forces that are difficult to compensate in real time. Without developing a force-feedback system, these effects can be eliminated by routing the tendons or wires through the axes of rotation in the wrist. In a one DOF wrist, wires can be routed along the axis of rotation without experiencing tension. Figure 7(b) shows that if a second DOF is added then the wires must be routed about both axes of rotation (a single point) to avoid unwanted forces. It is difficult to achieve this in practice since there are over 20 wires, each with a diameter of 0.5 mm. The solution in our design was to route the wires as close to the center of rotation as possible to help eliminate these effects. Figure 7(c) shows a close up view of the artificial carpal tunnel. The acrylic ring serves to guide the wires as well as connect the palm to the forearm by acting as the center of the universal joint. The forearm creates six separate entrance locations to the carpal tunnel which reduces friction between the wires.

### *2.4. Graphical comparison to the human hand*

It is important to quantitatively compare the design similarity of the DART hand to the human and other robotic hands. Factors included in the comparison include weight (with actuators), number of fingers (including thumb), DOF per finger and wrist, number of sensor types and fingertip force. DOF per finger means adding every DOF, including the thumb, and dividing by the number of fingers. The wrist is included in this calculation because it considerably amplifies the manipulation capabilities of the hand and is essential to many of the hand's useful actions. The equation used is shown below:

$$\left(\frac{\text{No. of fingers}}{5}\right)\left(\frac{(\text{DOF/finger}) + (\text{DOF/wrist})}{7}\right) \times \left(\frac{\text{No. of sensor types}}{6}\right)\left(\frac{\text{fingertip force}}{50.9\ \text{N}}\right)\left(\frac{15\ \text{N}}{\text{weight}}\right). \quad (1)$$

The numbers used for the human hand come from several sources. Clauser *et al* [25] reported that the mean mass of a male right hand is ~0.4 kg and the forearm mass is 1.13 kg leading to a combined mass of 1.53 kg which is 15 N. Astin [26] has reported the mean strength of the index finger to be 50.9 N. Human hands have six different types of sensors: tactile, pressure, temperature, muscle force, muscle position and joint position [23]. Figure 8 shows the comparative

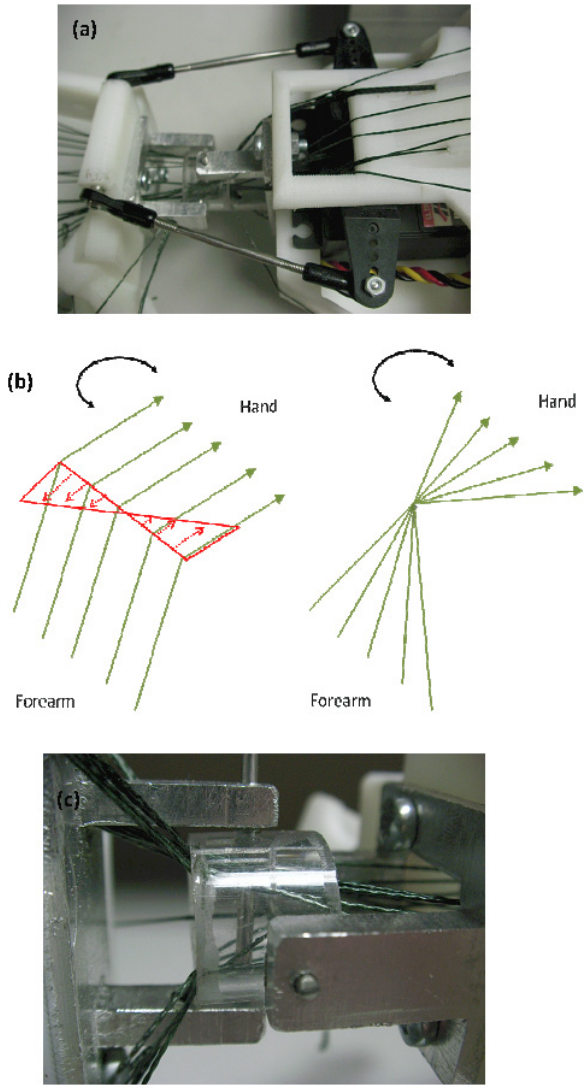


**Figure 7.** (a) Wrist mechanism utilizing two servo motors and a differential system that rotates about a universal joint. (b) Tension forms in wires that are not routed about each axis of rotation. The green arrows represent wires and the red arrows represent tension profiles. (c) Artificial carpal tunnel which guides the wires to the hand.

analysis using equation (1) for various hands reported in the literature and table 1 lists the parameters for these hands. The graph does not entirely convey anthropomorphism since it is possible to exceed human performance in sensor types, and fingertip force or weight. Thus, it is more a quantification of functional potential since as the numerical value increases so does the number of actions that can be successfully performed by the hand. Two different values are given for each hand: with and without a three DOF wrist. This is done to show how the wrist affects the numerical scores since most robotic hands in the literature do not feature a wrist or forearm mechanism. Figure 8 shows that the DART hand has exceptional functional potential compared to other artificial hands. Including more sensor types would be the best area of improvement to increase the performance of the DART hand.

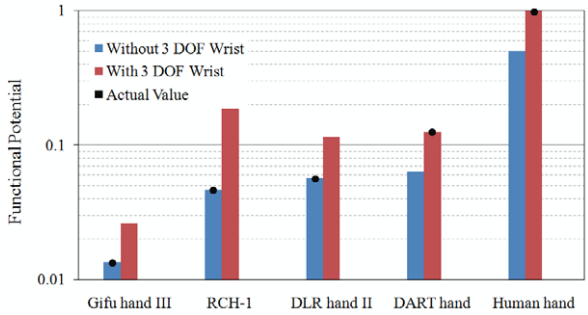


**Figure 8.** Functional potential comparison of the DART hand and other hands reported in the literature to the human hand. Black dots represent actual values of the full mechanical systems reported in the literature.

## 3. Kinematics and control

### *3.1. Control methodology*

The objective of this project is to design and optimize the performance of a humanoid hand for typing. Typing and piano playing are often considered to be among the more complex forms of skilled serial action performed by human beings [23] and therefore serve as suitable benchmarks in the development of a humanoid hand. Several systems reported in the literature have deployed complex control strategies. The DRL-HIT-Hand [6] utilizes 12 sensors per finger including joint torque and position, motor position, fingertip force and temperature. This hand has demonstrated playing music, autonomously grasping a bottle and tele-operation. A piano playing robot, developed by Huh *et al* [27], utilizes 21 degrees of freedom and an inverse kinematic approach to play music. Edin *et al* [28] have used on–off contact sensors as well as a custom-made triaxial force sensor based on strain gauges to compare the different dynamic stages of the hand while lifting objects. Various other robotic grippers have been developed that perform grasping, lifting and certain dexterous tasks, but to our knowledge there are currently no robotic hands capable of accurately typing on a keyboard at human speed. In this study, we utilize a closed-loop control strategy based on motor and joint position as well as fingertip pressure. The next iteration of this artificial hand will include tension sensors on the wires for redundancy in force-feedback control.

Figure 9(a) shows a flow diagram of the control strategy. The input text can come from a voice recognition program or through a keyboard. The word(s) to be typed are separated by character and assigned to a finger using standard keyboard finger placements. Motor commands are then sent to the motors to hover above the desired key before pressing. After the key is pressed, MATLAB checks to see if this was the desired key. If the pressed key was not the desired key then the hand will hit the delete button, adjust itself accordingly and try again. If the pressed key was the desired key, the program checks to see if it is the last character in the array. If it is the last character then the program ends; if not, then the next desired key is loaded and the cycle starts again. The Denavit–Hartenberg method was used to develop a spatial relationship between each joint. Since the joints in the DART hand have a

**Table 1.** Parameter list of robotic hands reported in literature.

| Name | No. of fingers | Wrist DOF | Finger DOF | Weight (g) | Fingertip force (N) | Sensors |
|---|---|---|---|---|---|---|
| DLR hand II | 4 | N/A | 3 | 1800 | 10 | Joint/motor position, joint/fingertip torque, temperature, accelerometers |
| Gifu hand III | 4 | N/A | 3.25 | 1400 | 3.4 | Tactile, motor/joint position |
| RCH-1 | 5 | N/A | 1 | 920 | 15 | Fingertip force, tactile, joint/motor position |
| DART hand | 4 | 3 | 3 | 1530 | 14.4 | Joint/motor position, fingertip force |

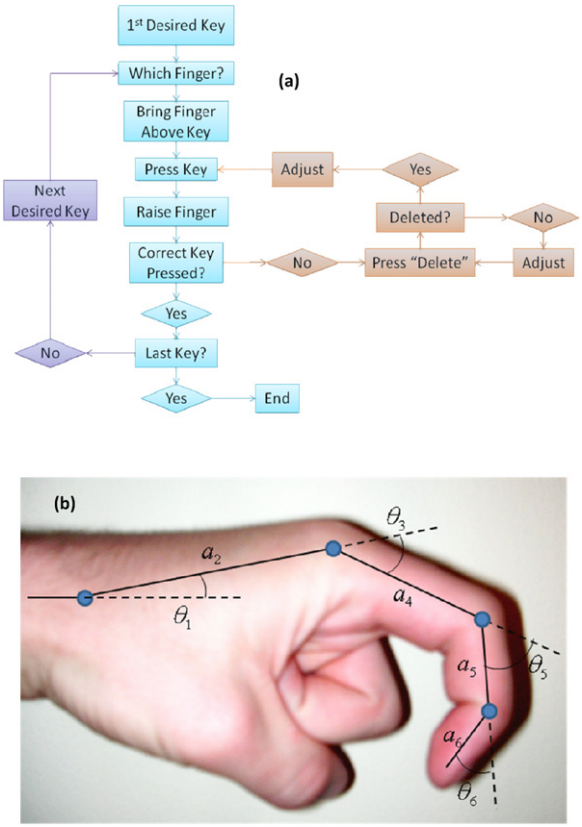


**Figure 9.** (a) Control strategy flow diagram, and (b) DH link and angle labels.

stationary axis of rotation, unlike the human hand, this method is suitable for creating a kinematic model. The DH method is very attractive in robotics because it makes complex positional calculations of multi-link systems simple by arranging them into a set of rotational and translational matrices [29]. If one were to imagine their right hand on a keyboard, ready to type, the global reference frame would be located at the center of rotation of the wrist. The $x$-axis points toward the left hand, the $y$-axis points away from the keyboard and the $z$-axis points toward the screen. The matrices below represent rotation about the $z$ and $x$-axis, respectively:

$$\begin{bmatrix} \cos(\theta) & -\sin(\theta) & 0 & 0 \\ \sin(\theta) & \cos(\theta) & 0 & 0 \\ 0 & 0 & 1 & 0 \\ 0 & 0 & 0 & 1 \end{bmatrix}$$

$$\begin{bmatrix} 1 & 0 & 0 & 0 \\ 0 & \cos(\alpha) & -\sin(\alpha) & 0 \\ 0 & \sin(\alpha) & \cos(\alpha) & 0 \\ 0 & 0 & 0 & 1 \end{bmatrix}.$$

**Table 2.** Link parameters for wrist to fingertip.

| Link | $a$ | $\alpha$ | $d$ | $\theta$ |
|---|---|---|---|---|
| 0 | 0 | −90 | 0 | $\theta_0$ |
| 1 | 0 | −90 | 0 | $\theta_1$ |
| 2 | $a_2$ | 90 | 0 | $\theta_2$ |
| 3 | 0 | −90 | 0 | $\theta_3$ |
| 4 | $a_4$ | 90 | 0 | $\theta_4$ |
| 5 | $a_5$ | 0 | 0 | $\theta_5$ |
| 6 | $a_6$ | 0 | 0 | $\theta_6$ |

In order to find the end effector position in a linkage system where the reference frame rotates about the $z$-axis then the $x$-axis, the two matrices above have to be multiplied. The last column of the product then gives equations for the $x$, $y$ and $z$ position (top to bottom) of the end effector with respect to the global axis. In the DART hand, there are seven joints which means that seven rotational matrices need to be multiplied together which produces a $4 \times 4$ matrix with large equations for the $x$, $y$ and $z$ position. Further details on the DH method and its derivation can be found in [29]. Link parameters for the DH convention are provided in table 2 and the schematic in figure 9(b) is labeled accordingly. The notation $\theta_0$ corresponds to rotation of the wrist, $\theta_2$ to wrist abduction/adduction and $\theta_4$ corresponds to MP joint abduction/adduction and cannot be shown in figure 9 since the rotation is in a plane perpendicular to the figure.

### 3.2. Redundancy

Since the key position is the desired location of the fingertip, an inverse kinematic analysis was performed to determine joint angles in the kinematic chain from wrist to fingertip. An issue commonly encountered while modeling complex biological systems is redundancy, which leads to an infinite combination of joint angles that create the desired output and requires additional constraining equations to solve each joint angle. There are six degrees of freedom between the wrist and fingertip. Since the IP joints are coupled with a four-bar mechanism, five of the joint angles need to be solved leaving one joint which can be geometrically calculated. The IP joint angles and fingertip trajectory of the DART hand can be accurately represented ($R$ value greater than 0.98) with the following relationship [13, 30, 31]:

$$\theta_{\mathrm{DIP}} = (2/3)\,\theta_{\mathrm{PIP}} \tag{2}$$

$$\theta_6 = (2/3)\,\theta_5. \tag{3}$$

This simple relationship was derived to simplify kinematic calculations which helped in decreasing the simulation time in MATLAB.

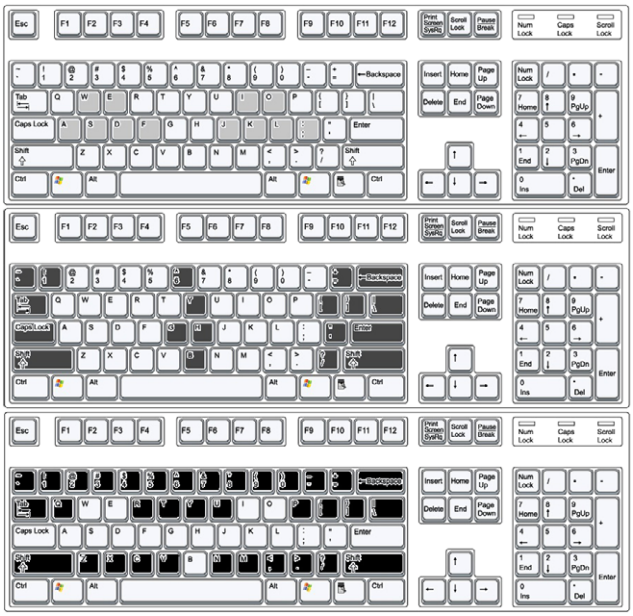

**Figure 10.** Keys that can be pressed in different wrist positions. Light grey—neutral wrist position, grey—abducted/adducted wrist position, Black—flexed/extended wrist position.

Breaking down the number of possible wrist positions into a finite number of set positions solves for $\theta_1$ and $\theta_2$. The third degree of freedom, $\theta_0$, was determined, through observation, to be 15°. Since there is currently no elbow or shoulder used for the positioning, the hand and forearm have to be properly positioned before typing. To do this, the locations of the keys with respect to the wrist had to be mapped out beforehand. Figure 10 shows the different keys that can be pressed while the wrist flexes, extends, adducts and abducts. The keys colored blue in this figure can be pressed while the wrist is in the neutral position. The keys colored red can be pressed while the wrist adducts and abducts and the keys colored green can be pressed while the wrist flexes and extends from its neutral position. Some of the keys are colored twice, which means that the wrist must rotate about two axes to reach them.

The degree of freedom in the MP joint (knuckle) responsible for adduction/abduction, $\theta_4$, was solved next. Figures 11(a) and (b) show that orientation of the palm and finger affects the trajectory of the fingertip on the keyboard. If the plane of the palm was parallel with the plane of the keyboard, the geometry would be simple. But since $\theta_0$ exists, the '$X$' location of the key must be adjusted. Equation (4) was developed using simple trigonometric relationships to solve for adduction/abduction ($\theta_4$).

$$\theta_4 = 90 - \tan^{-1}\left(\frac{Y}{X - X_{\text{shift}}}\right) \tag{4}$$

$$X_{\text{shift}} = Z_{\text{MP}} \tan\theta_0. \tag{5}$$

This process determines a suitable $\theta_4$ that lines up the finger with the desired key in the $X$–$Y$ plane and enables a two-dimensional analysis of the remaining degrees of freedom in a new reference frame ($YY$–$ZZ$). In this new two-dimensional coordinate system, $YY$ represents the axial location of the key with respect to the finger and $ZZ$ represents the distance between the MP joint and the key perpendicular to the $YY$ axis, as shown in figure 11(c). The minimum distance, $L$, between the MP joint (knuckle) and the desired key can be found because the locations of the knuckle and key with respect

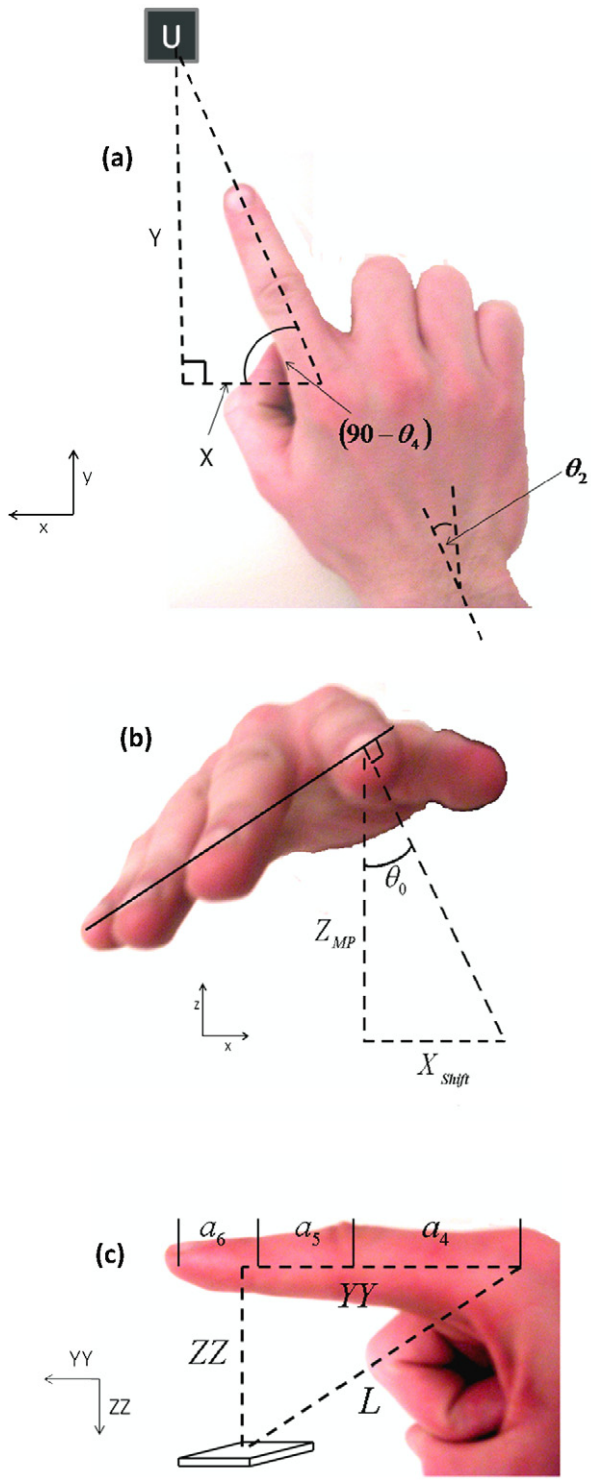


**Figure 11.** (a) $X$–$Y$ plane view of a hand in the global reference frame, (b) $X$–$Z$ plane view of a hand in the global reference frame, and (c) $YY$–$ZZ$ plane view in the 'new' coordinate system.

to the wrist are known in the global reference frame ($X$–$Y$–$Z$). The relevant expressions are given below:

$$L = \sqrt{(X_{\mathrm{MP}} - X_{\mathrm{KEY}})^2 + (Y_{\mathrm{MP}} - Y_{\mathrm{KEY}})^2 + (Z_{\mathrm{MP}} - Z_{\mathrm{KEY}})^2} \quad (6)$$

$$X_{\mathrm{MP}} = a_2\cos(\theta_0)\sin(\theta_2) - a_2\cos(\theta_2)\sin(\theta_0)\sin(\theta_1) \quad (7)$$

$$Y_{\mathrm{MP}} = a_2\sin(\theta_0)\sin(\theta_2) + a_2\cos(\theta_0)\cos(\theta_2)\sin(\theta_1) \quad (8)$$

$$Z_{\mathrm{MP}} = a_2\cos(\theta_1)\cos(\theta_2). \quad (9)$$

Now, as we try to solve for the $YY$ and $ZZ$ components of the finger length in the new coordinate system, two equations can be formulated using simple geometry:

$$L_{YY} = a_4\cos(\theta_3) + a_5\cos(\theta_5) + a_6\cos((2/3)\theta_5) \quad (10)$$

$$L_{ZZ} = a_4\sin(\theta_3) + a_5\sin(\theta_5) + a_6\sin((2/3)\theta_5). \quad (11)$$

The Pythagorean theorem can now be used to set these two equations equal to $L$:

$$L = \sqrt{L_{YY}^2 + L_{ZZ}^2}. \quad (12)$$

$\theta_3$ and $\theta_5$ are then solved, since there is only one combination of these angles that will reach the desired key position.

### *3.3. Closed-loop calibration and performance*

The human body is a closed-loop proprioceptive system that is affluent to recognizing and responding to disturbances. Open-loop control is a suitable approach in robotics as long as the task does not require any reaction to external stimuli and the system is resistant to disturbances or creep. For example, if the artificial hand received an overzealous high-five, the wires could stretch and cause position errors if no sensors were in place to tell it otherwise. Even over time the wires may lose some of their tension and cause similar errors. For these reasons it is important to have sensors in place that keep track of joint position. Analog Hall effect sensors (part number 785-SS496A from Mouser Electronics) were chosen for this purpose due to their small size and ease of mounting. The sensors were mounted in the four-bar linkage between the PIP and DIP joints shown in figure 12(a). An example signal from the PIP joint Hall sensor during 90° of travel is shown in figure 12(a). The signal peaks ranged from 805 mV to 816 mV for the PIP joint while the signal ranged from 812 to 816 mV for the DIP joint due to the difference in mounting orientations. Pressure sensors (Tekscan ZFLEXA201-25) capable of measuring forces up to 25 lbs were placed at each fingertip in order to provide feedback as to when a key has been sufficiently pressed. Figure 12(b) shows the data taken while a human subject types 'the quick brown fox jumped over the lazy dog'. Each peak represents when the index finger hits a key and has a peak force range from 0.78 to 1.1 N. This sensor is utilized to stop the MP joint from flexing once it reads a force value greater than 0.6 N so that the finger does not continue into the keyboard after the key is struck.

All of the transformation matrices from the DH model as well as sensor inputs and outputs were run through MATLAB. The joint angles were solved and then converted into motor commands which are then sent to the controller through a serial port. With the current code architecture a typing speed of 20 words min$^{-1}$ is achieved using only the right hand. With the addition of a left hand, a typing speed of over 30 words min$^{-1}$ is anticipated. Figures 13(a)–(d) show the prototype hand reaching different keys. While typing, the 19 motors experienced a peak current of 2.7 A with a total average power consumption of ∼6.4 W. Table 3 provides a summary of the characteristics of the DART hand and highlights its excellent performance given the cost-effective design of this hand.

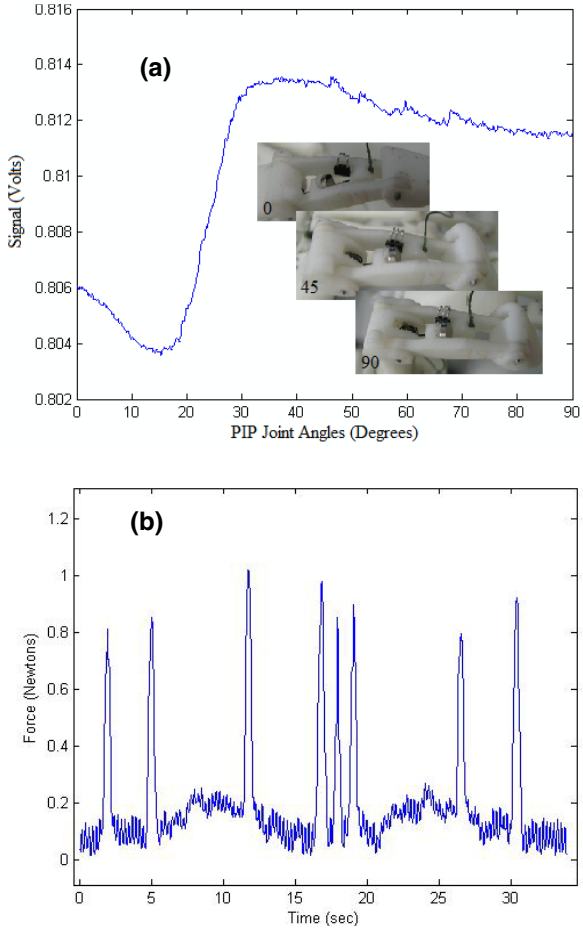


**Figure 12.** (a) Example signal acquired from the Hall effect sensor in the PIP joint showing the magnet and sensor positions at 0°, 45° and 90°. (b) Example signal acquired from the fingertip pressure sensor while typing a full sentence.

## 4. Conclusions and future work

In this study, the biomimetic design and performance of a 19 DOF robotic humanoid hand, the DART hand, was presented. Similarities between human joints and robot joints were highlighted in terms of basic functional characteristics such as independent joint and finger control, range of motion, output forces, weight and speed. Another important characteristic in this design was maintaining the human form because tasks such as tying shoes, holding mugs, opening doors and typing

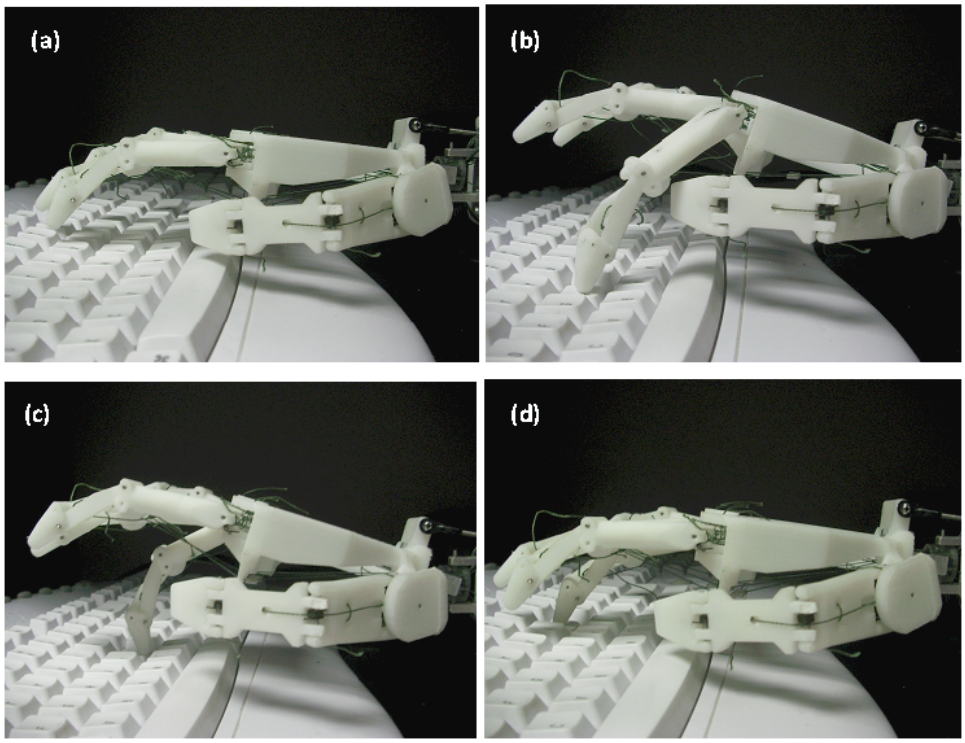


**Figure 13.** (a)–(d) The DART hand typing, from top left to bottom right, 'Y' 'H' 'L' 'O'.

**Table 3.** Summary of humanoid and average human hand characteristics.

| | DART hand | Human (male) |
|---|---|---|
| Hand size (mm) | 180 × 90 × 50 | 189 × 84 × 48 |
| Forearm size (mm) | 315 × 100 × 85 | 275 × 88 × 75 |
| Hand weight (kg) | 0.09 | 0.40 |
| Forearm weight (kg) | 0.96 | 1.13 |
| Degrees of freedom | 19 | 23 |
| Joint ranges of motion (DIP, PIP, MP) (deg) | 70, 90, 90 | 70, 110, 90 |
| Grasp speed (s) | 0.35 | 0.15 |
| Fingertip force (N) | 15 | 50.9 |
| Typing speed (words $min^{-1}$) | 20 | 33 |

on keyboards are tailored for human hands. An underactuated finger design utilizing a four-bar mechanism was optimized using ADAMS to create a fingertip trajectory similar to that of a human. A three DOF wrist was developed that allowed servo-driven wires to pass to the palm while minimizing unwanted tensional forces due to rotation. A forearm was designed to house 19 motors and electronics while retaining human size and weight. A kinematic model was developed using the Denavit–Hartenberg method and was used to eliminate system redundancy and perform an inverse kinematic analysis to achieve proper joint angles while typing. A closed-loop control strategy was implemented which included feedback about motor positions, joint angles and fingertip force. Future work will include integrating cable tension, temperature and tactile sensors into the design and embedding them in a silicone skin which will cover the mechanical structure.

## Acknowledgments

The authors gratefully acknowledge the financial support from ICTAS and NSF INAMM program.

## References

[1] Carrozza M C, Cappiello G and Micera S 2006 Design of a cybernetic hand for perception and action *Biol. Cybern.* **9** 629–44

[2] Bell C 1834 *The Hand; Its Mechanism and Vital Endowments as Evincing Design* (London: William Pickering)

[3] Kawasaki H, Komatsu T and Uchiyama K 2002 Dexterous anthropomorphic robot hand with distributed tactile sensor: Gifu hand II *IEEE/ASME Trans. Mechatronics* **2** 296–303

[4] Jacobsen S C *et al* 1984 The UTAH/M.I.T. dextrous hand: work in progress *Int. J. Robot. Res.* **3** 21–50

[5] Caffaz A *et al* 2000 The DIST-Hand, an anthropomorphic fully sensorized dexterous gripper *IEEE Conf. on Humanoids (Boston, MA)*

[6] Liu H *et al* 2007 The modular multisensory DLR-HIT-hand *Mech. Mach. Theory* **42** 612–25

[7] Zollo L *et al* 2007 Biomechatronic design and control of an anthropomorphic artificial hand for prosthetic and robotic applications *IEEE/ASME Trans. Mechatronics* **12** 418–29

[8] Folgheraiter M and Giuseppina G 2000 Blackfingers: an artificial hand that copies human hand in structure, size and functions *IEEE Conf. on Humanoids*

[9] Diftler M A and Ambrose R O 2001 Robonaut: a robotic astronaut assistant *6th Int. Symp. on Artificial Intelligence and Robotics and Automation in Space (Quebec)*

[10] Tadesse Y, Grange R W and Priya S 2009 Synthesis and cyclic force characterization of helical polypyrrole actuators for artificial facial muscles *Smart Mater. Struct.* **18** 1–17

[11] Thayer N and Shashank P 2010 Design and implementation of dexterous robotic hand for human controlled interfaces: a

comparative analysis with EAP systems *Proc. SPIE (San Diego, CA)* vol 7642
[12] Napier J 1993 *Hands* (Princeton, NJ: Princeton University Press)
[13] Controzzi M, Cipriani C and Carrozza C 2008 Mechatronic design of a transradial cybernetic hand *IEEE/RSJ Int. Conf. on Intelligent Robots and Systems (Nice)*
[14] O'Neill P A 1994 Myoelectric signal characteristics from muscles in residual upper limbs *IEEE Trans. Rehabil. Eng.* **2** 266–70
[15] Rodrigues-Cheu L E and Casals A 2006 Sensing and control fo a prosthetic hand with myoelectric feedback *1st IEEE/RAS-EMBS Int. Conf. on Biomedical Robotics and Biomechatronics (Pisa)*
[16] Zhao J *et al* 2006 A five-fingered underactuated prosthetic hand control scheme *1st IEEE/RAS-EMBS Int. Conf. on Biomedical Robotics and Biomechatronics (Pisa)*
[17] Chang L Y and Matsuoka Y 2006 A Kinematic Thumb Model for the ACT Hand *Proc. of IEEE International Conf. on Robotics and Automation (Orlando)* pp 1000–5
[18] Cabas R, Cabas L M and Balaguer C 2006 Optimized design of the underactuated robotiic hand *IEEE Int. Conf. on Robotics and Automation (Orlando)*
[19] Park I W *et al* 2005 Mechanical design of humanoid robot platform KHR-3 (KAIST Humanoid Robot-3: HUBO) *Proc. 5th IEEE-RAS Int. Conf. on Humanoid Robots* pp 321–6
[20] Rhee C *et al* 2004 Door opening control using the multi-fingered robotic hand for the indoor service robot *IEEE Int. Conf. on Robotics and Automation (New Orleans)*
[21] Zhang W, Chen Q and Sun Z 2004 Passive adaptive grasp multi-fingered humanoid robot hand with high under-actuated function *IEEE Int. Conf. on Robotics and Automation (New Orleans)*
[22] Fukaya N *et al* 2000 Design of the TUAT/Karlsruhe humanoid hand *IEEE/RSJ Int. Conf. on Intelligent Robots and Systems*
[23] Jones L A and Lederman J J 2006 *Human Hand Function* (New York: Oxford University Press)
[24] Henry Dreyfuss Associates 2002 *The Measure of Man and Woman: Human Factors in Design* (New York: Wiley)
[25] Clauser C E, McConville J T and Young J W Weight, volume and center of mass of segments of the human body *(AMRL TR 69-70). Wright-Patterson Air Force Base (Ohio)* (NTIS No. AD-T10 622)
[26] Astin A D, Maury A, Karl H E and Wojcik L 1999 Finger force capability: measurement and prediction using anthropometric and myoelectric measures *Thesis* submitted to the Faculty of the Virginia Polytechnic Institute and State University in partial fulfillment of the requirements for the degree of Master of Science in Industrial and Systems Engineering, Blacksburg, VA
[27] Huh S *et al* 2007 Development of a piano-playing robot system *11th Int. Conf. on Mechatronics Technology (Ulsan)* pp 5–9
[28] Edin B B *et al* 2006 A bio-inspired approach for the design and characterization of a tactile sensory system for a cybernetic prosthetic hand *IEEE Int. Conf. on Robotics and Automation (Orlando)*
[29] Spong M W and Vidyasagar M 1989 *Robot Dynamics and Control* (New York: Wiley)
[30] ElKoura G and Singh K 2003 Handrix: animating the human hand *Eurographics/SIGGRAPH Symp. on Computer Animation*
[31] Lin J, Wu Y and Huang T S 2001 Modeling the constraints of human hand motion *Proc. 5th Annual Federated Laboratory Symp.*
[32] Zupan M, Ashby M F and Fleck N A 2002 Actuator classification and selection-the development of a database *Adv. Eng. Mater.* **4** 933–40